# GBT-BASED STRUCTURAL ANALYSIS OF THIN-WALLED MEMBERS: OVERVIEW, RECENT PROGRESS AND FUTURE DEVELOPMENTS

**D. Camotim[1], N. Silvestre[1], R. Gonçalves[2] and P.B. Dinis[1]**
[1]*Civil Engineering Department, ICIST/IST, Technical University of Lisbon, Av. Rovisco Pais, 1049-001 Lisboa, Portugal*
*E-mail: dcamotim@civil.ist.utl.pt*
[2]*EST Barreiro, Polytechnical Institute of Setúbal, Rua Stinville 14, 2830-114 Barreiro, Portugal*

## Abstract

This paper provides an overview of the Generalised Beam Theory (GBT) fundamentals and reports on the novel formulations and applications recently developed at the TU Lisbon: the use of conventional GBT to derive analytical distortional buckling formulae and extensions to cover (i) the buckling behaviour of members with ($i_1$) branched, closed and closed/branched cross-sections and ($i_2$) made of orthotropic and elastic-plastic materials, and (ii) the vibration and post-buckling behaviours of elastic isotropic/orthotropic members. In order to illustrate the usefulness and potential of the new GBT formulations, a few numerical results are presented and briefly discussed. Finally, some (near) future developments are briefly mentioned.

## 1. Introduction

Generalised Beam Theory (GBT) was first proposed by Richard Schardt in 1966 and has, since then, fostered a vast amount of theoretical and applied research activity at the University of Darmstadt. However, due to the fact that practically all publications originating from this research group were available exclusively in German (including the book published by Schardt in 1989), GBT had virtually no impact for non-German-speaking researchers up until the early 90s. This situation was altered by J.M. Davies, who learnt about GBT in the mid 80s and, almost single-handed, disseminated it among the English-speaking technical and scientific communities together with his Ph.D. students Leach and Jiang, Davies employed GBT to perform in-depth investigations on the buckling behaviour of cold-formed steel members and, in particular, showed that this approach is a valid and often advantageous alternative to finite element or finite strip analyses (Davies, 1998, 2000). Moreover, it appears that Davies can also be credited with encouraging Schardt to start publishing in English (Schardt, 1994a,b).

Although GBT has recently attracted considerable attention from several researchers around the world (e.g., Rendek and Baláž, 2004; or Simão and Silva, 2004), it seems fair to say that the vast majority of the novel formulations and applications originated from the Technical University of Lisbon – this can be attested by the review paper recently published by the authors (Camotim et al., 2004), which summarises the work carried out prior to 2004. Therefore, the objective of this work is to provide a follow-up of that paper, by (i) reporting on the research activity concerning GBT undertaken in the last couple of years and (ii) addressing the developments expected for the foreseeable future. At this stage, it should be pointed out that, due to space limitations, it is only possible (i) to provide a brief overview of the new findings, (ii) to present a very small number of illustrative examples and (iii) to mention the main references, where the interested reader may find much more detailed accounts of all these topics dealt with in this paper.



*M. Pandey et al. (eds), Advances in Engineering Structures, Mechanics & Construction,* 187–204

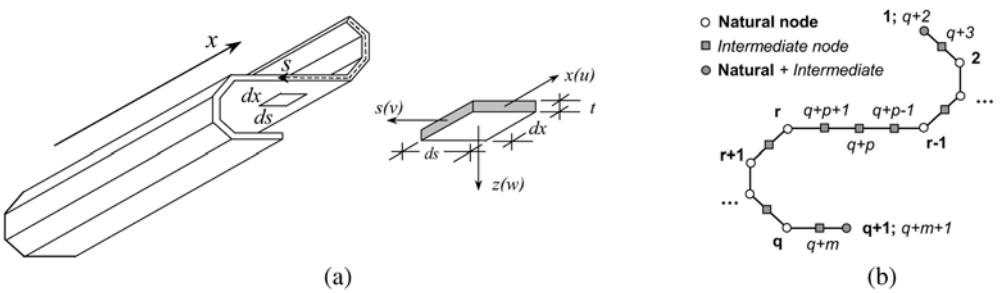


*Figure 1.* Thin-walled member (a) geometry, axes/displacements; (b) cross-section discretisation.

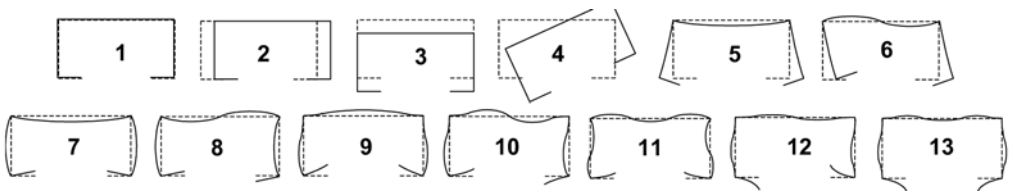


*Figure 2.* Lipped channel first thirteen deformation mode in-plane shapes.

### 1.1. *Conventional GBT*

In this paper, *conventional GBT* designates the formulation intended to perform stability (bifurcation) analyses of thin-walled members with unbranched (folded-plate) thin-walled members and made of linear elastic isotropic materials (e.g., most cold-formed steel profiles) – this designation stems from the fact that both (i) the vast majority of Schardt's publications and (ii) all of Davies's work concern members with these characteristics. Moreover, all the recently developed GBT formulations can be viewed, to a smaller or larger extent, as modifications or extensions of this conventional one.

A conventional GBT analysis involves (i) a *cross-section analysis*, leading to the GBT deformation modes and corresponding modal mechanical properties, and (ii) a *member linear stability analysis*, to obtain the member bifurcation stress resultants and associated buckling mode shapes (e.g., Davies, 1998; or Schardt, 1994a). In the case of the arbitrary $q$-walled member shown in Figure 1(a) and for the cross-section discretisation depicted in Figure 1(b) ($q + 1$ natural and $m$ intermediate nodes), the performance of the cross-section analysis leads to the system of $q + m + 1$ GBT equilibrium equations (one per deformation mode)

$$EC_{ik}\phi_{k,xxxx} - GD_{ik}\phi_{k,xx} + EB_{ik}\phi_k + W^{\sigma}_{j.o}X_{jik}\phi_{k,xx} = 0, \tag{1}$$

where (i) $(\cdot)_{,x} \equiv d(\cdot)/dx$, (ii) $\phi_k(x)$ are modal amplitude functions, (iii) $E, G$ are Young's and shear moduli, (iv) $W^{\sigma}_{j.o}$ are uniform (usually single-parameter) pre-buckling stress resultants and (v) the various matrix/tensor components are related to the cross-section stiffness ($C_{ik}$, $D_{ik}$, $B_{ik}$) and geometric effects ($X_{jik}$). Together with its boundary conditions, system (1) defines a standard eigenvalue problem, the solution of which (i) can be obtained by means of several standard methods (e.g., finite differences, finite elements or Galerkin's method) and (ii) yields the member bifurcation stress resultants and buckling modes. The latter are combinations of the GBT deformation modes, illustrated in Figure 2 for the case of a lipped channel cross-section ($q = 5$ and $m = 7$).

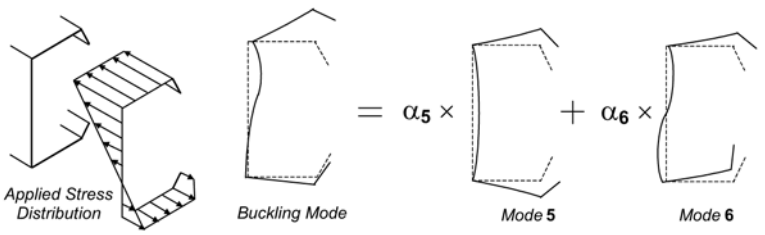


*Figure 3.* Lipped channel member buckling mode as a linear combination of modes **5** and **6**.

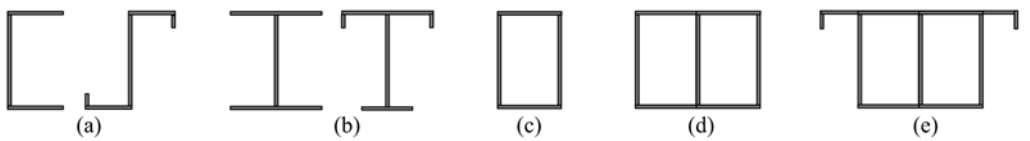


*Figure 4.* (a) Unbranched open, (b) branched open, (c) unbranched closed, (d) branched closed and (e) arbitrary branched open/closed thin-walled cross-sections.

### 1.2. *Recent Developments*

The novel GBT applications and formulations addressed in this paper concern (i) the development of *distortional buckling formulae* (using the conventional GBT), (ii) the *buckling analysis* of members ($ii_1$) with arbitrary cross-section shapes (branched and/or closed multi-cell) and ($ii_2$) made of isotropic/orthotropic elastic or isotropic elastic-plastic materials, (iii) the *vibration* analysis of isotropic/orthotropic elastic folded-plate members (loaded or unloaded) and (iv) the *post-buckling* analysis of isotropic/orthotropic elastic folded-plate members. This sequence is kept in the presentation and the various applications and/or formulations are grouped according to the type of structural analysis (buckling, vibration or post-buckling).

## 2. Buckling Analysis

### 2.1. *Distortional Buckling Formulae*

Since GBT allows for the possibility of performing approximate buckling analyses including any number of deformation modes, one may develop analytical formulae providing accurate distortional buckling stress estimates for lipped channel, $Z$-section and rack-section columns, beams and beam-columns with several support conditions (Silvestre and Camotim, 2004a,b). These formulae are obtained through *symbolic* GBT-based bifurcation analyses that include only either *one* (columns) or *two* (beams and beam-columns) cross-section distortional deformation modes: modes **5** (symmetric) and **6** (anti-symmetric) in Figure 3, where this procedure is illustrated for the case of lipped channel members. Extensive parametric studies showed that the buckling stress estimates provided by the GBT-based formulae (i) are consistently accurate and (ii) always compare favourably with the values yielded by formulae previously developed by other authors.

### 2.2. *Cross-Section Shape*

The cross-section of a thin-walled member is classified according to its mid-line, which may be (i) *open* or *closed* and (ii) *branched* or *unbranched* (see Figure 4). As mentioned earlier, the conventional GBT is valid only for folded-plate members, i.e., members with open unbranched cross-sections. Thus, in order to extend its application to all other cross-section shapes, one must modify

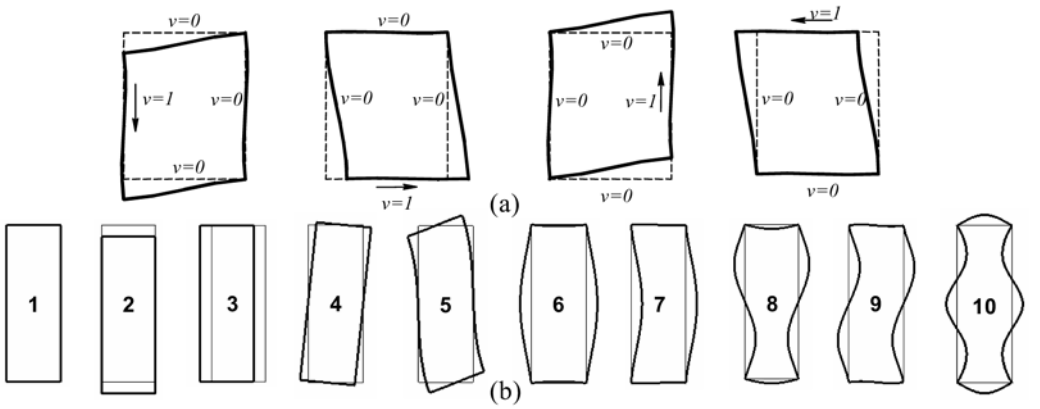


*Figure 5.* (a) Determination of the additional deformation modes accounting for shear deformation and (b) the 10 most relevant deformation modes of a narrow rectangular hollow cross-section.

the cross-section analysis procedure – since the member analysis remains unaltered, both system (1) and its boundary conditions retain their *forms*. This task has now been completed for any conceivable cross-section shape and comprised the following three stages:

(i) The first extension concerned (unbranched) single-cell closed cross-sections and involves the inclusion of four *additional* deformation modes, which ($i_1$) are related to the *shear deformation* of the cross-section mid-line and ($i_2$) stem from the imposition of unit transverse displacements in each wall, while preventing all the other ones, as shown in Figure 5(a) (Gonçalves and Camotim, 2004a). Moreover, one must incorporate the term $\int_s G t v_i v_j ds$ in the analysis, to account for the virtual work associated with the shear strains. The 10 most relevant deformation modes of a narrow rectangular hollow section are displayed in Figure 5(b) and one notices that, besides the global (**1**–**4**) and local-plate (**6**-**10**) modes, similar to the ones yielded by the conventional GBT, a novel *distortion* (not *distortional*) mode **5** appears – together with mode **4**, it models the cross-section shear deformation (Gonçalves and Camotim, 2004b).

(ii) Next, a methodology that can handle arbitrarily branched open cross-sections was developed, thus overcoming difficulties related to ($ii_1$) the proper selection of the elementary warping and flexural functions and ($ii_2$) the solution of the statically indeterminate folded-plate problem (Dinis et al., 2006). One must view the cross-section as a combination of an unbranched sub-section and an ordered sequence of branches, which leads to the straightforward identification of the *dependent natural nodes*, i.e., the natural nodes where the warping displacements cannot be imposed (they must be *calculated*) – the number of such nodes is equal to $\sum(m_{wi} - 2)$, with the summation extending to all branching nodes and $m_{wi}$ being the number of walls emerging from branching node $i$. These concepts are illustrated in Figure 6, where ($ii_1$) the cross-section depicted in Figure 6(a) has six dependent nodes (see Figure 6(e)) and ($ii_2$) two possible combinations of an unbranched sub-section and the corresponding branch sequence are displayed in Figures 6(b)–(d) (note that in both cases one must go up to second-order branches).

(iii) Finally, Gonçalves et al. (2006) have just developed the "definitive" formulation, in the sense that it is applicable to fully arbitrary cross-sections, namely those combining closed cells with open branches. A brief description of the steps and procedures involved in this formulation is presented next and illustrated through the cross-section depicted in Figure 7(a): an I-shaped section with closed cells separating the web from the unequal flanges – it has 13 walls, 2 closed cells and 12 natural nodes (6 branching ones):

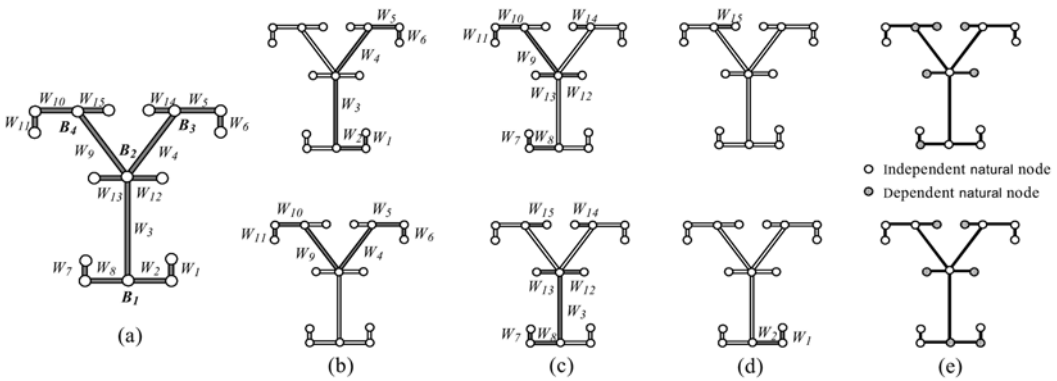


*Figure 6.* Illustrative branched section (a) geometry and two possible (b) unbranched sub-sections, (c) first-order branches, (d) second-order branches and (e) independent/dependent natural nodes.

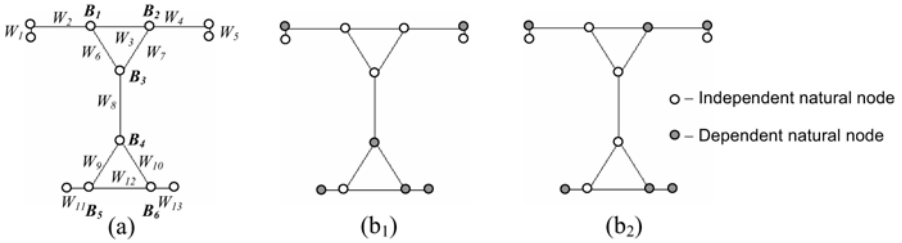


*Figure 7.* (a) Cross-section geometry and (b) dependent and independent natural nodes.

(iii.1) Choice of the dependent natural nodes – Figures 7($b_1$)–($b_2$) show two possible choices for the 6 dependent and 6 independent natural nodes to be considered in the analysis.

(iii.2) Determination of the "warping initial shape functions", by imposing elementary functions at each independent natural node and assuming that Vlassov's hypothesis holds in all walls, i.e., following the methodology developed by Dinis et al. (2006).

(iii.3) Determination of the "local-plate initial shape functions", by imposing elementary flexural functions at each intermediate node – 13 intermediate nodes were included in the illustrative example (mid-points of each internal wall and free ends of the external ones).

(iii.4) Identification of the conventional *deformation modes*, yielded by the simultaneous diagonalisation of the stiffness matrices $[C_{ik}]$ and $[B_{ik}]$. In the case of the illustrative example, one identifies 19 deformation modes, 11 of which are shown in Figure 8: 5 warping (**2**–**6**) and 6 local-plate (**13**–**18**) – note that modes **2**–**4** are "rigid-body" ones and mode **1** (axial extension) has been omitted.

(iii.5) Sequential imposition of unit membrane shear strains in each wall belonging to a closed cell, keeping all remaining walls free of those strains, and determination of the corresponding "initial shear shape functions". In the example, 6 unit shear strains are imposed (3 per closed cell), by combining $u$ and $v$ displacements – enforcing these unit strains may be a quite cumbersome task and some guidelines on how to carry it out can be found in the work by Gonçalves et al. (2006).

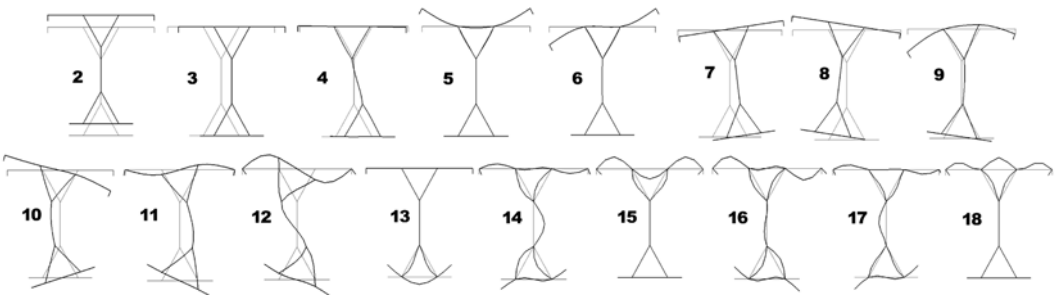


*Figure 8.* In-plane shapes of the 17 most relevant warping (**2–6**), shear (**7–12**) and local-plate (**13–18**) modes.

(iii.6) Identification of the *shear deformation modes*, again by simultaneously diagonalising matrices $[C_{ik}]$ and $[B_{ik}]$[1] – in this case, one obtains the 6 shear deformation modes (**7–12**) shown in Figure 8.

### 2.3. *Material Behaviour*

A GBT formulation applicable to members made of materials other than isotropic and linear elastic requires modifications that depend on the specific type of material behaviour.[2] This task has been carried out for (i) *orthotropic* linear elastic materials (e.g., laminated plate fibre-reinforced plastics – FRP) and (ii) isotropic *non-linear elastic-plastic* materials (e.g., stainless steel or aluminium). In the former case, first addressed about four years ago (Silvestre and Camotim, 2002), the layer (lamina) *plane-stress* constitutive law reads

$$\begin{Bmatrix} \sigma_{xx} \\ \sigma_{ss} \\ \sigma_{xs} \end{Bmatrix} = \begin{bmatrix} \bar{Q}_{11} & \bar{Q}_{12} & \bar{Q}_{13} \\ \bar{Q}_{12} & \bar{Q}_{22} & \bar{Q}_{23} \\ \bar{Q}_{13} & \bar{Q}_{23} & \bar{Q}_{33} \end{bmatrix} \begin{Bmatrix} \varepsilon_{xx} \\ \varepsilon_{ss} \\ \gamma_{xs} \end{Bmatrix}, \tag{2}$$

where $\bar{Q}_{ij}$ are "transformed reduced stiffness components" depending on the layer (i) fibre and plastic matrix material properties and (ii) fibre orientation (Jones, 1999). Moreover, the mechanical behaviour of a laminated plate member also varies with its layer properties and configuration (Silvestre and Camotim, 2002). In the most general case (arbitrary orthotropy, i.e., anisotropy), the GBT system (1) becomes

$$C_{ik}\phi_{k,xxxx} + H_{ik}\phi_{k,xxx} - D_{ik}\phi_{k,xx} + F_{ik}\phi_{k,x} + B_{ik}\phi_k - X_{jik}W^{\sigma}_{j,0}\phi_{k,xx} = 0 \tag{3}$$

and its boundary conditions must be modified accordingly. It is worth noting (i) the additional tensors $H_{ik}$ and $F_{ik}$, accounting for material coupling effects between torsion and longitudinal/transversal flexure, and (ii) that, due to the layer-variation of the material properties, the various tensor components are now *mechanical properties* – material constants and geometrical characteristics fused together. Another aspect that deserves to be mentioned is the need to include in the analysis deformation modes that take into consideration the non-linearity of the warping displacement variation within the width of each wall and, therefore, are also associated with membrane shear strains, i.e., do not satisfy Vlassov's assumption (Silvestre and Camotim, 2004c; Silvestre, 2005). The warping

[1] Since the conventional and shear modes are not identified jointly, the overall matrices $[C_{ik}]$ and $[B_{ik}]$ are not diagonal – only their principal sub-matrices exhibit this property.

[2] Although most of the novel GBT formulations have not yet been applied to other than isotropic and linear elastic members, this is a straightforward (even if time-consuming) task that is planned for the near future.

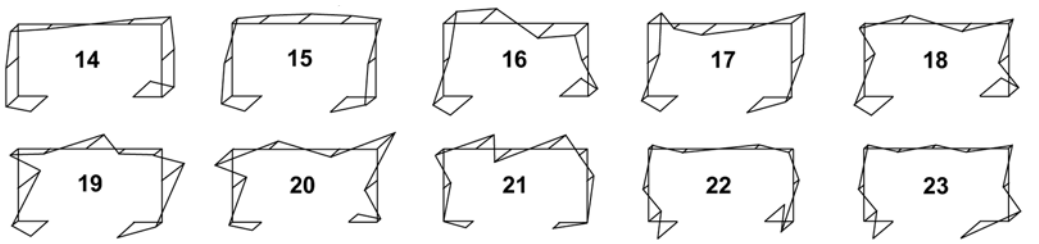


*Figure 9.* Lipped channel ten most relevant shear modes associated with non-linear warping.

configurations of this set of additional shear deformation modes are shown in Figure 9, for the case of a lipped channel cross-section.

Concerning the buckling analysis of isotropic non-linear elastic-plastic members, one begins by recalling that, if no strain reversal occurs along the fundamental equilibrium path, an elastic-plastic solid and its "hypoelastic comparison solid" have identical critical bifurcation stresses/loads (Hill, 1958). Thus, by (i) monitoring the evolution of the instantaneous moduli (on the fundamental path) and (ii) adopting *incremental* constitutive relations, it is possible to determine the member plastic bifurcation behaviour using non-linear elastic stability theory. For fundamental states with only longitudinal normal stresses, the plane-stress incremental constitutive relations read

$$\begin{Bmatrix} \dot{\sigma}^B_{xx} \\ \dot{\sigma}^B_{ss} \\ \dot{\sigma}^B_{xs} \end{Bmatrix} = \begin{bmatrix} \dot{E}_{11} & \dot{E}_{12} & 0 \\ \dot{E}_{21} & \dot{E}_{22} & 0 \\ 0 & 0 & \dot{G} \end{bmatrix} \begin{Bmatrix} \dot{\varepsilon}^B_{xx} \\ \dot{\varepsilon}^B_{ss} \\ \dot{\gamma}^B_{xs} \end{Bmatrix}, \qquad \dot{\sigma}^M_{xx} = E_T \dot{\varepsilon}^M_{xx}, \tag{4}$$

where (i) $\dot{\sigma}_{ij}$ and $\dot{\varepsilon}_{ij}$ are stress-rate and strain-rate components, (ii) $\dot{E}_{ij}$ and $\dot{G}$ are the instantaneous elastic and shear moduli, (iii) $E_T$ is the longitudinal uniaxial tangent modulus and (iv) $(\cdot)^B$ and $(\cdot)^M$ are superscripts identifying bending and membrane terms. The material uniaxial stress-strain law is commonly described by Ramberg–Osgood type expressions (Rasmussen, 2003) and, due to the well-known "plate plastic buckling paradox" (Hutchinson, 1974), *both* $J_2$-deformation and $J_2$-flow small strain plasticity theories were included in the GBT formulation (Gonçalves and Camotim, 2004, 2005). After the incorporation of the instantaneous moduli, the hypoelastic bifurcation analysis leads to the system of *incremental* GBT equations

$$C_{ik}\dot{\phi}_{k,xxxx} - D_{ik}\dot{\phi}_{k,xx} + B_{ik}\dot{\phi}_k + X_{ik}\dot{\phi}_{k,xx} = 0 \tag{5}$$

and associated boundary conditions, where (i) functions $\dot{\phi}_k$ provide the deformation mode amplitude rates and (ii) all tensor components are *load-dependent* through the instantaneous moduli (Gonçalves and Camotim, 2005). Note that (5) is applicable to rather general (uniaxial-stress) loading conditions – the only restriction is that they must satisfy the basic hypothesis of Hill's "comparison solid" concept: the material behaviour may be assumed as hypoelastic in the close vicinity of the bifurcation point (Hill, 1958; Hutchinson, 1974).

## 3. Vibration Analysis

Given the well-know mathematical similarity between the stability (bifurcation) and *vibration* eigenvalue problems, the derivation of a GBT vibration formulation constitutes a relatively easy task: it suffices to replace the geometric effects by their *dynamic* counterparts, as done by Schardt and Heinz (1991) for isotropic linear elastic members, and by Silvestre and Camotim (2004d), for *orthotropic*

linear elastic laminated plate members. Very recently, these authors proposed a novel combined formulation that makes it possible to analyse the vibration behaviour of *loaded* orthotropic members (Silvestre and Camotim, 2005a,b). In this case, the GBT system of equilibrium equations reads

$$(\mathcal{K}_{ik} + W_m^0 \mathcal{G}_{ik} - \omega^2 \mathcal{M}_{ik})\phi_k + (\mathcal{K}_{ij} - \omega^2 \mathcal{M}_{ij})\varphi_j = 0, \tag{6}$$

$$(\mathcal{K}_{hk} - \omega^2 \mathcal{M}_{hk})\phi_k + (\mathcal{K}_{hj} - \omega^2 \mathcal{M}_{hj})\varphi_j = 0, \tag{7}$$

and corresponds to the assembly of two subsystems, both including coupling components – while the first is associated with the *conventional* modes (see Figure 2 – amplitudes $\phi_k$), the second is related to the *shear* modes (see Figure 9 – amplitudes $\varphi_j$). The system is expressed in terms of differential operators concerning *linear stiffness* ($\mathcal{K}_{ik}$, $\mathcal{K}_{ij}$, $\mathcal{K}_{hk}$, $\mathcal{K}_{hj}$), *geometric stiffness* ($\mathcal{G}_{ik}$) and mass ($\mathcal{M}_{ik}$, $\mathcal{M}_{ij}$, $\mathcal{M}_{hk}$, $\mathcal{M}_{hj}$) effects. The boundary conditions include generalised *normal* and *shear* stress resultants, involving terms that stem from (i) normal stress equilibrium and (ii) the variation of the shear stresses along the cross-section wall thickness. For composite members displaying cross-ply orthotropy (the case of the illustrative example presented in Section 6.2) the system (6)–(7) may be rewritten in matrix form as (Silvestre and Camotim, 2005a,b)

$$\begin{aligned}&(\mathbf{C_c}\phi_{,xxxx} - \mathbf{D_c}\phi_{,xx} + \mathbf{B_c}\phi + \mathbf{C_{cs}}\,\boldsymbol{\varphi}_{,xxx}) - \xi_B W_m^0(\mathbf{X_{c}}_{,m}\phi_{,xx})\\ &\quad - \xi_V \omega^2(\mathbf{R_c}\phi - \mathbf{Q_c}\phi_{,xx} + \mathbf{Q_{cs}}\,\boldsymbol{\varphi}_{,x}) = \mathbf{0},\end{aligned} \tag{8}$$

$$(\mathbf{C_{sc}}\phi_{,xxx} + \mathbf{C_s}\,\boldsymbol{\varphi}_{,xx} - \mathbf{D_s}\,\boldsymbol{\varphi}) - \xi_V \omega^2(\mathbf{Q_{sc}}\phi_{,x} + \mathbf{Q_s}\,\boldsymbol{\varphi}) = \mathbf{0}, \tag{9}$$

where (i) the subscripts $(\cdot)_\mathbf{c}$, $(\cdot)_\mathbf{s}$ and $(\cdot)_\mathbf{cs}$ stand *conventional*, *shear* and coupling *conventional-shear* mode quantities, and (ii) the various dynamic stiffness matrices $R_{ik}$ and $Q_{ik}$ account for the effects of mass forces related to the *in* and *out-of-plane* cross-section translations, rotations and translation-rotation couplings. By making (i) $\xi_B = 1$ and $\xi_V = 0$, (ii) $\xi_B = 0$ and $\xi_V = 1$ or (iii) $\xi_B = \psi (0 < \psi \leq 1)$ and $\xi_V = 1$, this system defines linear eigenvalue problems associated with (i) buckling analyses, (ii) a free vibration analyses of load-free members and (iii) free vibration analyses of loaded members – in the last case, the loads $W_m^0$ are known *a priori* and $\omega^2$ are the problem eigenvalues.

## 4. Post-Buckling Analysis

A previously developed and numerically implemented non-linear GBT formulation to analyse the post-buckling behaviour of initially imperfect isotropic linear elastic folded-plate members (Silvestre and Camotim, 2003) was recently extended to encompass orthotropic FRP composite members (Silvestre and Camotim, 2004e; Silvestre, 2005). This involved major modifications with respect to the conventional GBT, namely (i) to employ the stress-strain relations given in (2) and (ii) to consider the non-linear strain-displacement relations

$$\begin{aligned}\varepsilon_{xx} &= u_{,x} + \frac{1}{2}(v_{,x}^2 + w_{,x}^2) - z w_{,xx} - \bar{u}_{,x} - \frac{1}{2}(\bar{v}_{,x}^2 + \bar{w}_{,x}^2) + z\bar{w}_{,xx},\\ \varepsilon_{ss} &= v_{,s} + \frac{1}{2}(v_{,s}^2 + w_{,s}^2) - z w_{,ss} - \bar{v}_{,s} - \frac{1}{2}(\bar{v}_{,s}^2 + \bar{w}_{,s}^2) + z\bar{w}_{,ss},\\ \gamma_{xs} &= u_{,s} + v_{,x} + v_{,x}v_{,s} + w_{,x}w_{,s} - 2z w_{,xs} - \bar{u}_{,s} - \bar{v}_{,x} - \bar{v}_{,x}\bar{v}_{,s} - \bar{w}_{,x}\bar{w}_{,s} + 2z\bar{w}_{,xs},\end{aligned} \tag{10}$$

where the bars identify the terms associated with the initial imperfections. Moreover, one must also include an additional set of *transverse extension* deformation modes in the cross-section analysis,

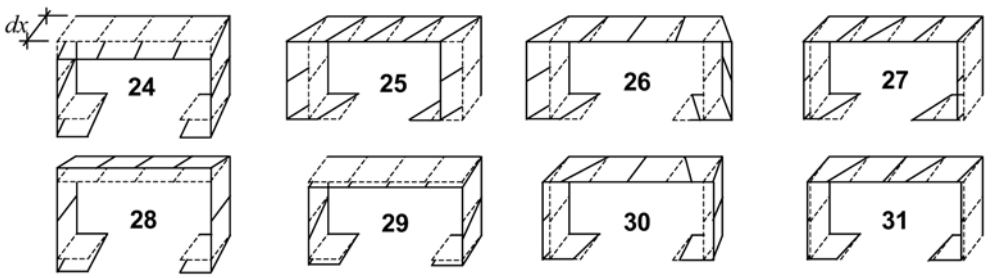


*Figure 10.* Lipped channel eight most relevant transverse extension modes.

which (i) account for the "bowing effect" stemming from the transverse bending of cross-section walls and (ii) do not comply with Vlassov's assumption – they stem from the sequential imposition of unit transverse and null warping displacements at both the natural and intermediate nodes. The configurations of the eight most relevant transverse extension deformation modes of a lipped channel cross-section are displayed in Figure 10.

After (i) incorporating (10) into the principle of virtual work, (ii) performing several operations, described in detail elsewhere (Silvestre and Camotim, 2003; Silvestre, 2005) and (iii) including the *special* cross-section analysis, one is led to the member equilibrium equations, written variationally as

$$\delta U_1 + \delta U_2 + \delta U_3 - \delta \bar{U}_1 - \delta \bar{U}_2 - \delta \bar{U}_3 + \delta \Pi_q + \delta \Pi_w = 0, \tag{11}$$

where (i) the strain energy terms $\delta U_1, \delta U_2$ and $\delta U_3$ are linear, quadratic and cubic functionals of the mode amplitude functions $\phi_i$, (ii) their "bar counterparts" contain the imperfection amplitude functions $\bar{\phi}_i$ and (iii) the $\delta\Pi$ terms stand for the virtual work done by distributed or concentrated external loads.

## 5. Numerical Implementation

The solution of the buckling and vibration eigenvalue problems is obtained by means of either (i) Rayleigh–Ritz's or Galerkin's method, in the case of simply supported members, i.e., members with locally and globally pinned and free-to-warp end sections, or (ii) a GBT-based beam finite element formulation that uses Hermitean cubic polynomials to approximate the buckling/vibration modes, for members with other end support conditions (Camotim et al., 2004; Silvestre, 2005; Gonçalves and Camotim, 2005; Dinis et al., 2006). As for the solution of system (11), it requires the development of another (non-linear) GBT-based beam finite element (also using Hermite and Lagrange cubic polynomials to approximate $\phi_k(x)$ and $\varphi_j(x)$) and resorting to an incremental-iterative numerical technique to determine the member equilibrium path (Silvestre and Camotim, 2003; Silvestre, 2005). After the usual integrations, the FEM system of algebraic equations reads

$$(\mathbf{K}_0^{(e)} + \mathbf{K}_1^{(e)} + \mathbf{K}_2^{(e)})\mathbf{d}^{(e)} - (\mathbf{K}_0^{(e)} + \bar{\mathbf{K}}_1^{(e)} + \bar{\mathbf{K}}_2^{(e)})\bar{\mathbf{d}}^{(e)} = \mathbf{f}_{\mathbf{e}}^{(e)}, \tag{12}$$

where (i) $\mathbf{K}_p^{(e)}$ are linear ($p = 0$) and non-linear ($p = 1, 2$) *secant* stiffness matrices, (ii) $\mathbf{d}^{(e)}$, and $\bar{\mathbf{d}}^{(e)}$ are the vectors of generalised and initial imperfection nodal displacements and (iii) $\mathbf{f}_e^{(e)}$ is the external applied force vector. The well-known Newton–Raphson predictor-corrector iterative technique was employed to determine the member post-buckling equilibrium paths (e.g., Crisfield, 1991–1996).

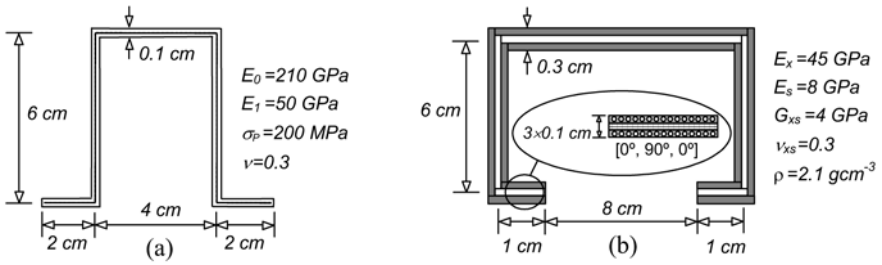


*Figure 11.* Geometrical and material properties: (a) buckling and (b) vibration and post-buckling.

## 6. Illustrative Examples

In order to illustrate the application and potential of the above GBT formulations, some numerical results are presented and briefly discussed next. Even if buckling, vibration and post-buckling results are included here, the space limitations make it impossible to cover more than a small fraction of the different (i) features outlined earlier and (ii) possibilities offered by the various GBT analyses. All the relevant geometrical and material properties of the thin-walled members analysed are given in Figures 11(a)–(b) – note that the elastic-plastic uniaxial stress-strain law is described by a bi-linear expression. For validation purposes, some GBT-based linear elastic results are compared with FEM-based values yielded by the codes ADINA (Bathe, 2003) or ABAQUS (HKS, 2002) and adopting fine shell element member discretisations.

### 6.1. *Buckling*

The results shown in Figures 12(a)–(b) and 13(a)–(b) concern the bifurcation behaviour of isotropic elastic and elastic-plastic hat-section beams (uniform major axis bending) with end sections that are locally and globally pinned and may warp freely (Gonçalves and Camotim, 2005). While Figure 12(a) shows the 9 most relevant deformation modes (out of 15 – the cross-section discretisation involved the following intermediate nodes: 3 in each web, 1 in the flange mid-point and 1 in each stiffener free end), Figure 12(b) depicts three GBT-based buckling curves, corresponding to elastic and elastic-plastic ($J_2$-flow and $J_2$-deformation) beams and providing the variation of the critical moment $M_{\rm cr}$ with the normalised length $L/h$ (logarithmic scale). In addition, the white dots in Figure 12(b) stand for FEM-based elastic critical moments obtained using the code ADINA (Bathe, 2003).[3] As for Figures 13(a)–(b), they make it possible to compare the ADINA (perspective) and GBT-based (in-span cross-section) elastic critical buckling mode shapes of the beams indicated in Figure 12(b): lengths $L/h = 5$ (six-wave local-plate buckling modes $\mathbf{7+9}$) and $L/h = 10$ (single-wave distortional-flexural-torsional buckling modes $\mathbf{3+4+6}$). Although an in-depth discussion of the results shown in these two figures is beyond the scope of this paper, the following general comments and remarks are appropriate:

(i) The linear elastic $M_{\rm cr}$ values yielded by the GBT-based analyses practically coincide with the ones obtained using ADINA. Moreover, one notices that the critical buckling mode nature varies with $L/h$ as follows: (i) local-plate buckling (modes $\mathbf{7+9}$) for short beams ($L/h \leq 8.8$), (ii) distortional-flexural-torsional buckling (modes $\mathbf{3 + 4 + 6}$) for intermediate beams ($8.8 \leq$

[3] No validation is presented for the elastic-plastic GBT-based results, as the authors know no commercial FEM code capable of calculating plastic bifurcation moments – e.g., neither ADINA (Bathe, 2003) nor ABAQUS (HKS, 2002) offer such possibility.

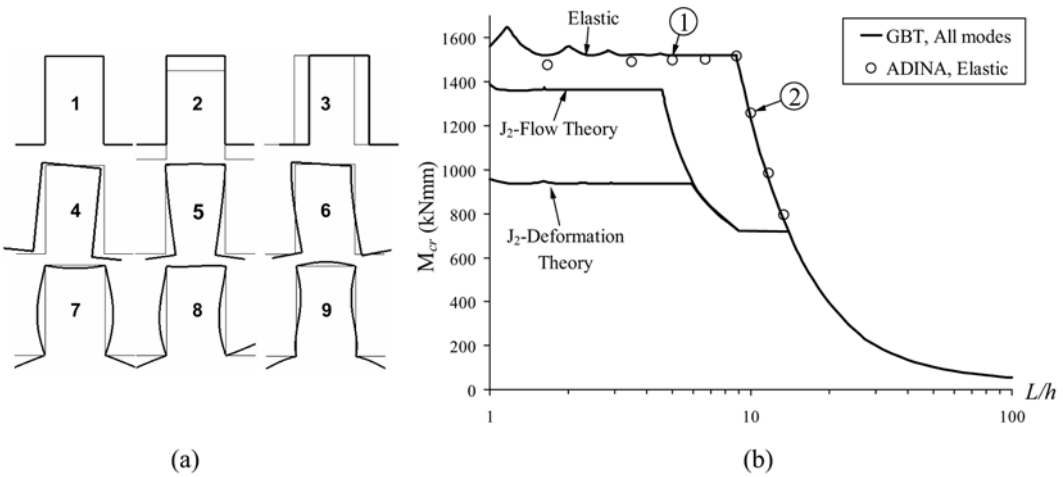


*Figure 12.* (a) Hat-section first 9 deformation mode shapes and (b) beam elastic and elastic-plastic $M_{\text{cr}}$ vs. $L/h$ curves (GBT-based and ADINA results).

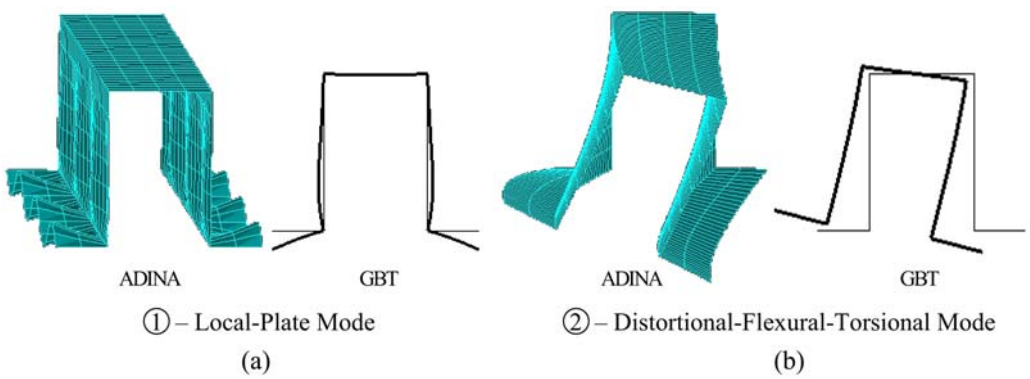


*Figure 13.* ADINA and GBT-based elastic critical buckling mode shapes – beams with (a) $L/h = 5$ and (b) $L/h = 10$.

$L/h \leq 20$) and (iii) "classical" lateral-torsional buckling (modes **3** + **4**) for the longer beams ($L/h \geq 20$). Finally, note that the accuracy of the ADINA results deteriorate for $L/h < 4$ (local-plate buckling), due to the occurrence of stress concentrations in the shell element model (in the vicinity of the end sections) – obviously, they lower the $M_{\text{cr}}$ values.

(ii) There is also a virtual coincidence between the elastic critical buckling mode shapes yielded by GBT and ADINA obviously, the former concern the most deformed beam cross-sections.

(iii) The elastic-plastic GBT-based results confirm the well-known fact that deformation theory leads to lower critical buckling loads than flow theory. This is particularly true for local-plate buckling, which involves almost exclusively transverse plate bending – recall that the transverse plate bending stiffness $t^3 \dot{E}_{22}/12$ decreases more rapidly for deformation theory (Gonçalves and Camotim, 2004b). The differences are much less relevant for distortional-flexural-torsional buckling and vanish for lateral-torsional buckling (the beams buckle elastically). Due to higher local-plate buckling stresses, the length interval related to critical distortional-flexural-torsional buckling is larger for flow theory than for deformation theory.

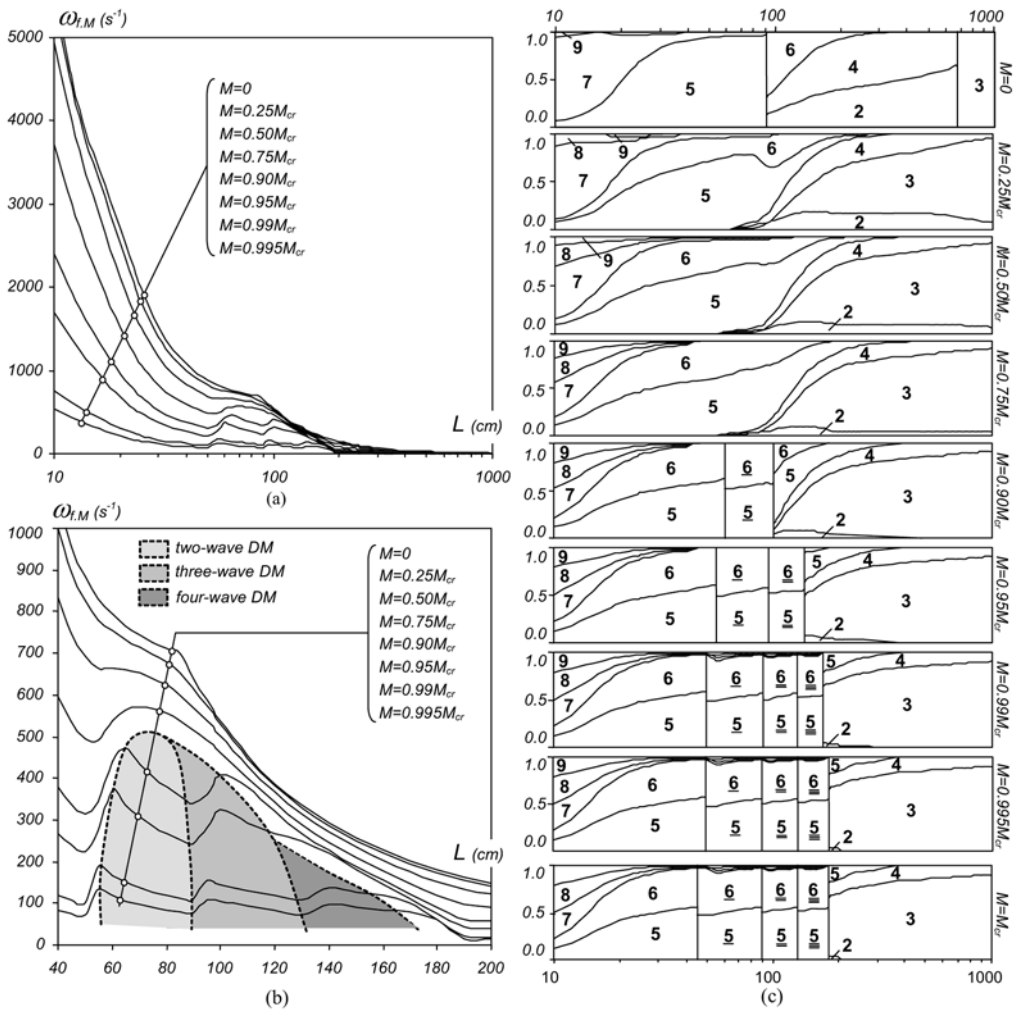


*Figure 14.* Variation of $\omega_f$, for (a) $10 < L < 1000$ cm and (b) $40 < L < 200$ cm, and (c) modal participation diagram of the beam fundamental vibration mode with $L$ and $M/M_{\mathrm{cr}}$.

## 6.2. *Vibration*

The vibration results shown in Figures 14(a)–(c) concern laminated plate lipped channel beams (members under uniform major axis bending) with (i) walls formed by three equally thick orthotropic layers made of identical FRP materials (epoxy resin reinforced with e-glass fibres) and exhibiting a cross-ply configuration [0°, 90°, 0°], (ii) locally/globally pinned and free-to-warp end sections and (iii) uniform mass density $\rho = 2.1$ gcm$^{-3}$ (Silvestre and Camotim, 2005a,b). The curves in Figure 14(a) show how the fundamental natural frequency $\omega_{f\cdot M}$ varies with the beam length $L$ (logarithmic scale) and bending moment ratio $M/M_{\mathrm{cr}}$ – the upper curve is related to the load-free member ($M = 0$) and is always associated with single-wave vibration modes ($\omega_{f\cdot 0} = \omega_{1\cdot 0}$).[4] The remaining seven curves correspond, in descending order, to increasing $M/M_{\mathrm{cr}}$ value – each

[4] Due to space limitations, the results concerning the buckling behaviour and load-free vibration behaviour of the beams cannot be presented here. The interested reader is referred to the recent works by Silvetre and Camotim (2005a,b).

curve is associated with a fixed percentage of $M_{cr}$, which varies with the beam length. Because $M_{cr}$ corresponds to buckling modes exhibiting several waves for 55 cm $< L <$ 180 cm, it is interesting to look more closely at the curves $\omega_{f \cdot M}(L)$ in this length range – thus, Figure 14(b) shows these curves for 40 cm $< L <$ 200 cm. Moreover, the modal participation diagrams shown in Figure 14(c) supply additional information about the contribution of the GBT deformation modes (see Figure 2) to the fundamental vibration modes of beams with nine $M/M_{cr}$ values.[5] Note that the presence of none, one, two or three bars underneath a mode number indicates a single, two, three or four-wave contribution to the vibration mode. The analysis of the results displayed in Figures 14(a)–(c) prompts following conclusions and/or comments:

(i) For $L <$ 55 cm or $L >$ 180 cm, the beams buckle in single-wave critical buckling modes (see footnote 4), which means that one has $\omega_{f \cdot M}(L) \equiv \omega_{1 \cdot M}(L)$ and all curves have fairly similar shapes. Moreover, it is worth pointing out that, although the beam fundamental vibration modes always exhibit a single wave, their shapes differ from those of the beam ($i_1$) critical buckling modes and ($i_2$) load-free fundamental vibration modes – indeed, the beam fundamental vibration mode shape "travels" between them as the ratio $M/M_{cr}$ increases (see Figure 14(c)). For instance, note that the participation of mode **2**, which contributes significantly to the load-free member *flexural-torsional* vibration modes, continuously decreases as $M/M_{cr}$ grows, until it vanishes for $M = M_{cr}$ – mode **2** is absent from the beam critical buckling mode (it appears in its pre-buckling path).

(ii) For 55 $< L <$ 180 cm, the beam critical buckling modes have more than one wave (see footnote 4) and the shapes of the curves $\omega_{f \cdot M}(L)$ become visibly different as the value of $M/M_{cr}$ increases, as clearly illustrated in Figure 14(b) – these curves ($ii_1$) cease to decrease monotonically and, for large enough $M/M_{cr}$ values, ($ii_2$) they are no longer "smooth", exhibiting sudden and quite pronounced slope reversals. Moreover, Figure 14(c) shows that the beam fundamental vibration mode wave number varies between one and the number of waves appearing in the beam critical buckling mode, as $M/M_{cr}$ grows – for $M \geq 0.90 M_{cr}$, the fundamental vibration mode successively exhibits 2, 3 and 4 waves (Figure 14(b) identifies very well the $L - M/M_{cr}$ combinations associated with each case). Apparently, the $M/M_{cr}$ value that triggers a non-single wave number depends on the percentage difference between $M_{cr}$ and $M_{b \cdot 1}$ (bifurcation moment leading to a single-wave buckling mode), i.e., a $M_{cr}/M_{b \cdot 1}$ decrease lowers the $M/M_{cr}$ value corresponding to the change (Silvestre and Camotim, 2005a,b).

(iii) Figure 14(c) shows that a beam with $L = 100$ cm vibrates in ($iii_1$) a flexural-torsional-distortional mode ($\mathbf{2+4+6}$) for $M = 0$, ($iii_2$) another flexural-torsional-distortional mode ($\mathbf{2+4+6+5}$) for $0 < M/M_{cr} < 0.3$, ($iii_3$) a single-wave distortional mode ($\mathbf{5+6}$) for $0.3 \leq M/M_{cr} < 0.8$ and ($iii_4$) similar two or three-wave distortional modes for $0.8 \leq M/M_{cr} < 0.9$ and $0.9 \leq M/M_{cr} \leq 1$, respectively. Since the combination of modes **5** and **6** attenuates the rotation of the tensioned flange-lip assembly and increases that of the compressed one (see Figure 2), it is possible to conclude that, for increasing $M/M_{cr}$ values, the amplitudes of the tensioned and compressed flange-lip motions tend to decrease and increase, respectively. Therefore, for moderate-to-high $M/M_{cr}$ values ($0.3 \leq M/M_{cr} < 1$), only the compressed flange-lip and the web upper half (due to compatibility) vibrate – they exhibit either 1, 2 or 3 waves (see the last two modes in Figure 15).

In order to validate the GBT-based results, some shell finite element analyses were carried out using the code ABAQUS (HKS, 2002) – they all involved beams with $L = 100$ cm and the results

[5] It was found that the shear modes associated with non-linear warping (see Figure 9) do not contribute to the beram fundamental vibration modes. Nevertheless, they were included in all analyses.

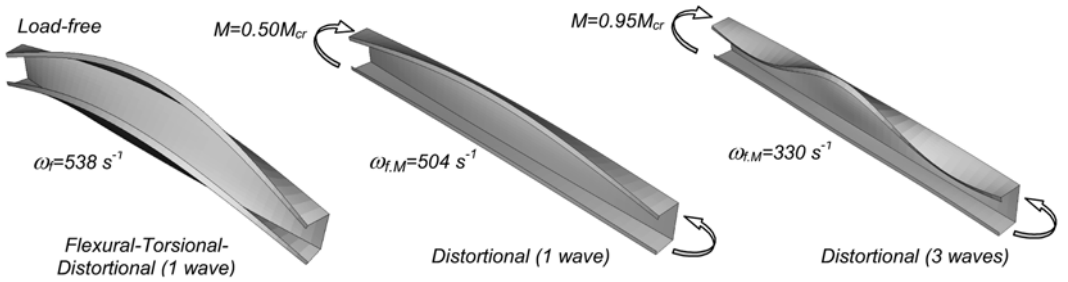


*Figure 15.* FEM-based beam fundamental frequencies and vibration mode shapes ($L = 100$ cm).

determined concerned $M/M_{b\cdot1} = 0.271, 0.407, 0.488, 0.516, 0.537, 0.543$ (the last ratio means $M = M_{\rm cr}$). The GBT and FEM-based $\omega_{f\cdot M}$ values read (i) $\omega_{f\cdot M} = 502, 463, 409, 325, 146, 0\ {\rm s}^{-1}$ (GBT) and (ii) $\omega_{f\cdot M} = 508, 487, 463, 418, 315, 268\ {\rm s}^{-1}$ (FEM), thus making it obvious that they become increasingly apart as $M/M_{b\cdot1}$ grows. In particular, note that, for $M = M_{\rm cr}$, GBT yields the (theoretically expected) *null* $\omega_{f\cdot M}$, while the FEM-based $\omega_{f\cdot M}$ value is about 50% of $\omega_{f\cdot0} = 538\ {\rm s}^{-1}$ (it only becomes null for $M = 1.0134 M_{\rm cr}$). It was subsequently found that this rather surprising discrepancies stem from the fact that the ABAQUS shell FEA incorporate the stiffening effect due to the primary (first-order) bending deflections, which is not taken into account by the developed GBT formulation. This fact was overcome by performing the FEM vibration analyses in "adequately pre-cambered beams" (Silvestre and Camotim, 2005a,b), thus enabling a meaningful comparison between the two sets of $\omega_{f\cdot M}$ values. Figure 15 shows the FEM-based fundamental vibration mode shapes and frequency values for beams with $L = 100$ cm acted by $M = 0$; 0.5; $0.9 M_{\rm cr}$ – the FEM values $\omega_{f\cdot0} = 530\ {\rm s}^{-1}$, $\omega_{f\cdot0.5} = 504\ {\rm s}^{-1}$ and $\omega_{f\cdot0.9} = 330\ {\rm s}^{-1}$ agree very well with the GBT ones $\omega_{f\cdot0} = 538\ {\rm s}^{-1}$, $\omega_{f\cdot0.5} = 502\ {\rm s}^{-1}$ and $\omega_{f\cdot0.9} = 325\ {\rm s}^{-1}$ (differences of 1.5, 0.3 and 1.5%).

### 6.3. *Post-Buckling*

The results presented here concern the distortional post-buckling behaviour of two identical FRP laminated plate lipped channel columns (i) having locally/globally pinned and free-to-warp end sections, (ii) with the material properties and cross-section dimensions displayed in Figure 11(b) (identical to the ones considered in the vibration analyses presented in the previous subsection), (iii) containing critical-mode initial geometrical imperfections with amplitudes $v_0 = \pm 0.15 \cdot t$ ($t$ is the wall thickness and $v_0$ is the outward/inward motion of the flange-lip corners at mid-span), (iv) with length $L = 40$ cm and (v) discretised into ($v_1$) 6 natural and 17 intermediate (5 in the web and flanges and 1 per lip) nodes and ($v_2$) 8 finite elements (Silvestre and Camotim, 2004e). It is worth noting that the adopted column geometry ensures that (i) bifurcation occurs in a single-wave distortional mode and that (ii) local-plate/distortional mode interaction effects are not relevant – the ratio between the minimum local-plate and distortional buckling loads is 1.6 (Silvestre and Camotim, 2004c).

Figure 16(a) shows the post-buckling equilibrium paths $\sigma/\sigma_{{\rm cr}\cdot D}$ vs. $v/t$ ($\sigma_{{\rm cr}\cdot D} = 38.6$ MPa is the column critical buckling load and $v$ is the additional outward/inward flange-lip motion) of the two columns, henceforth termed "outward" and "inward". Also included are the results yielded by the shell FEA performed in ABAQUS (HKS, 2002). Figure 16(b), on the other hand, displays diagrams that provide the contributions of the various GBT deformations modes (depicted in Figures 2, 9 and 10) to various column deformed configurations located along their equilibrium paths. Finally, Figure 16(c) provides the post-buckling evolution of the mid-span normal stress distribution along

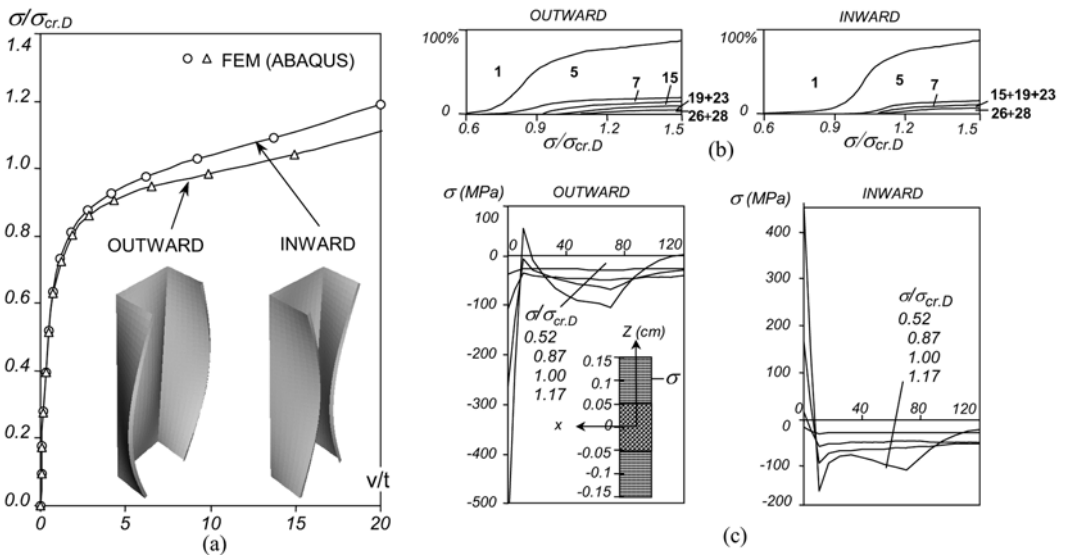


*Figure 16.* (a) Outward and inward column distortional post-buckling equilibrium paths $\sigma/\sigma_{\text{cr}\cdot D}$ vs. $v/t$, (b) diagrams providing the modal decomposition of the deformed configurations and (c) post-buckling evolution of the normal stress distribution $\sigma$ ($x = 20$ cm; $z = 0.1$ cm; $s$) for the outward and inward columns.

the mid-lines of the outward and inward column outer layers (longitudinally aligned fibres).[6] After a close observation of the above figures, one is led to the following conclusions:

(i) First of all, one instantly recognises the important role played by the initial imperfection "sign". Indeed, the inward column post-buckling stiffness and strength are larger than their outward column counterparts by a non-negligible amount. Like in the case of the isotropic members (Silvestre and Camotim, 2003), this distortional post-buckling *asymmetry* stems mostly from the different contributions of the shear modes **15** + **19** + **23** to the outward and inward column deformed configurations.

(ii) Then, attention should be drawn to the virtual coincidence between the GBT-based equilibrium paths and the post-buckling results yielded by ABAQUS. The fact that the GBT analyses never involved more than 450 degrees of freedom provides a clear assessment of the high computational efficiency of this approach. The corresponding (and similarly accurate) FEM results required the discretisation of the thin-walled columns by means of very refined shell element meshes.

(iii) In the initial pre-buckling stages, the normal stress distribution is uniform, since mode **1** dominates. As post-buckling progresses and regardless of the $v_0$ sign (outward or inward motions), the normal stress distribution becomes non-linear in the web and flanges, mostly due to the shear modes **15** + **19** + **23**.

(iv) In the outward column post-buckling stages, the contributions of modes **5** and **15** account for the fact that the compressive stresses ($\text{iv}_1$) increase near the web-flange node and ($\text{iv}_2$) decrease in the vicinity of the flange-lip corner. Moreover, for $\sigma/\sigma_{\text{cr}\cdot D} \geq 1.0$, tensile stresses start to develop around the flange-lip node and rather high compressive stresses appear close to the lip free ends. Conversely, the inward column exhibits a compressive stress increase near the flange-lip corner (all the flanges are under compression) and high tensile stresses develop in

[6] Due to symmetry, only one half of the normal stress distributions are represented in Figure 16(c).

the neighbourhood of the lip free ends – however, these tensile stresses are lower than the compressive ones appearing in the outward column. This last fact is due to the relevant participation of mode **19**, reinforcing mode 5 in the outward column and opposing it in the inward one.

## 7. Conclusion and Future Developments

After an extremely brief overview of the concepts/procedures involved in a "conventional" GBT analysis, the paper reported on the GBT formulations/applications recently developed at the TU Lisbon, namely:

(i) The use of "conventional GBT" to derive approximate analytical formulae to estimate distortional buckling stresses in lipped channel, zed-section and rack-section cold-formed steel members.
(ii) Extensions of the conventional GBT to cover members with ($ii_1$) arbitrary open/closed branched cross-sections and ($ii_2$) made of orthotropic linear elastic and non-linear elastic-plastic materials.
(iii) A GBT formulation to analyse the vibration behaviour of loaded folded-plate members made of orthotropic linear elastic materials.
(iv) A geometrically non-linear GBT formulation to analyse the post-buckling behaviour of folded-plate members made of orthotropic linear elastic materials.

To illustrate the application and provide an idea of the capabilities of the GBT approach to solve structural analysis problems, a few numerical results were presented and very briefly commented. For validation purposes, some of these results were also compared with values yielded by shell finite element analyses, performed in the commercial codes ADINA and ABAQUS.

Because a very rich research activity on GBT formulations, implementations and applications is still under way at the TU Lisbon, further developments are to be expected in the near-to-intermediate future. For instance, the topics being currently investigated include:

(i) GBT formulations to analyse the buckling behaviour of thin-walled members made of orthotropic linear elastic or non-linear elastic-plastic materials that exhibit arbitrary closed/branched cross-sections.
(ii) GBT formulations to analyse the vibration behaviour of thin-walled members made of orthotropic linear elastic materials and exhibiting arbitrary closed/branched cross-sections.
(iii) GBT formulations to analyse the buckling and vibration behaviour of isotropic linear elastic thin-walled members exhibiting arbitrary closed/branched cross-sections and subjected to non-uniform internal force and moment diagrams (i.e., under stress gradients).
(iv) GBT formulations to analyse the first and second-order behaviour of isotropic elastic-plastic thin-walled members with unbranched open cross-sections.
(v) A GBT formulation to analyse the post-buckling behaviour of orthotropic linear elastic thin-walled members with open branched and arbitrary closed/branched cross-sections.
(vi) The influence of local-plate/distortional and local/global mode interaction effects on the elastic post-buckling behaviour of cold-formed steel members.
(vii) The development of GBT-based beam finite elements intended to enable the performance of elastic first-order and buckling analyses of plane and spatial frames made of thin-walled steel members.

## References


Bathe, K.J./ADINA R&D Inc. (2003). *Adina System*.

Camotim, D., Silvestre, N., Gonçalves, R. and Dinis, P.B. (2004). GBT analysis of thin-walled members: new formulations and applications, in *Thin-Walled Structures: Recent Advances and Future Trends in Thin-Walled Structures Technology*, J. Loughlan (ed.), Canopus Publishing Ltd., Bath, pp. 137–168.

Crisfield, M. (1991–1996). *Nonlinear Finite Element Analysis of Solids and Structures: Essentials* (Vol. 1) and *Advanced Topics* (Vol. 2), John Wiley & Sons, Chichester.

Davies, J.M. (1998). Generalised beam theory (GBT) for coupled instability problems, in *Coupled Instability in Metal Structures: Theoretical and Design Aspects*, J. Rondal (ed.), Springer Verlag, Vienna, pp. 151–223.

Davies, J.M. (2000). Recent research advances in cold-formed steel structures, *Journal of Constructional Steel Research*, **55**(1–3), 267–288.

Dinis, P.B., Camotim, D. and Silvestre, N. (2006). GBT formulation to analyse the buckling behaviour of thin-walled members with arbitrarily 'branched' open cross-sections, *Thin-Walled Structures*, **44**(1), 20–38.

Gonçalves, R. and Camotim, D. (2004a). Buckling analysis of single and multi-cell closed thin-walled metal members using generalised beam theory, in *Proceedings of Fourth International Conference on Coupled Instabilities in Metal Structures* (CIMS'04, Rome, 27–29 September), pp. 119–130.

Gonçalves, R. and Camotim, D. (2004b). GBT local and global buckling analysis of aluminium and stainless steel columns, *Computers & Structures*, **82**(17–19), 1473–1484.

Gonçalves, R. and Camotim, D. (2005). Thin-walled member plastic bifurcation analysis using generalised beam theory, *Computers & Structures*, accepted for publication.

Gonçalves, R., Dinis, P.B. and Camotim, D. (2006). GBT linear and buckling analysis of thin-walled multi-cell box girders, in *Proceedings of SSRC Annual Stability Conference* (San Antonio, 8–11 February), pp. 329–352.

Hibbit, Karlsson and Sorensen Inc. (2002). *ABAQUS Standard* (Version 6.3).

Hill, R. (1958). A general theory of uniqueness and stability in elastic-plastic solids, *Journal of Mechanics and Physics of Solids*, **6**, 236–249.

Hutchinson, J.W. (1974), Plastic buckling, in *Advances in Applied Mechanics*, Vol. 14, C.S. Yih (ed.), Academic Press, New York, pp. 67–144.

Jones, R. (1999). *Mechanics of Composite Materials*, Taylor & Francis, Philadelphia.

Rasmussen, K.J.R. (2003). Full-range stress-strain curves for stainless steel alloys, *Journal of Constructional Steel Research*, **59**(1), 47–61.

Rendek, S. and Baláž, I. (2004). Distortion of thin-walled beams, *Thin-Walled Structures*, **42**(2), 255–277.

Schardt, R. (1966). Eine Erweiterung der technische Biegetheorie zur Berechnung prismatischer Faltwerke, *Stahlbau*, **35**, 161–171.

Schardt, R. (1989). *Verallgemeinerte technische Biegetheorie*, Springer Verlag, Berlin.

Schardt, R. (1994a). Generalised beam theory – an adequate method for coupled stability problems, *Thin-Walled Structures*, **19**(2–4), 161–180.

Schardt, R. (1994b). Lateral torsional and distortional buckling of channel and hat-sections, *Journal of Constructional Steel Research*, **31**(2–3), 243–265.

Schardt, R. and Heinz, D. (1991). Vibrations of thin-walled prismatic structures under simultaneous static load using generalized beam theory, in *Structural Dynamics*, W.B. Krätzig et al. (eds.), Balkema, Rotterdam, pp. 921–927.

Silvestre, N. (2005). *Generalised Beam Theory: New Formulations, Numerical Implementation and Applications*, Ph.D. Thesis in Civil Engineering, IST, Technical University of Lisbon [in Portuguese].

Silvestre, N. and Camotim, D. (2002). First and second-order generalised beam theory for arbitrary orthotropic materials, *Thin-Walled Structures*, **40**(9), 755–789 + 791–820.

Silvestre, N. and Camotim, D. (2003). Non-linear generalised beam theory for cold-formed steel members, *International Journal Structural Stability and Dynamics*, **3**(4), 461–490.

Silvestre, N. and Camotim, D. (2004a). Distortional buckling formulae for cold-formed steel C and Z-section members: Part I – derivation and Part II – validation and application, *Thin-Walled Structures*, **42**(11), 1567–1597 + 1599–1629.

Silvestre, N. and Camotim, D. (2004b). Distortional buckling formulae for cold-formed steel rack-section members, *Steel & Composite Structures*, **4**(1), 49–75.

Silvestre, N. and Camotim, D. (2004c). Influence of shear deformation on the local and global buckling behaviour of composite thin-walled members, in *Thin-Walled Structures: Advances in Research, Design and Manufacturing Technology* (ICTWS 2004, Loughborough, 22–24 June), J. Loughlan (ed.), Institute of Physics Publishing, Bristol, pp. 659–668.

Silvestre, N. and Camotim, D. (2004d). Generalised beam theory to analyse the vibration behaviour of orthotropic thin-walled members, in *Thin-Walled Structures: Advances in Research, Design and Manufacturing Technology* (ICTWS 2004, Loughborough, 22–24 June), J. Loughlan (ed.), Institute of Physics Publishing, Bristol, pp. 919–926.

Silvestre, N. and Camotim, D. (2004e). Generalised beam theory formulation to analyse the post-buckling behaviour of orthotropic laminated plate thin-walled members, in *Abstracts of 21st International Congress of Theoretical and Applied Mechanics* (ICTAM 04, Warsaw, 15–21 June), pp. 345–346.

Silvestre, N. and Camotim, D. (2005a). Local and global vibration behaviour of loaded folded-plate anisotropic members, in *Programme and Book of Abstracts of the Twelfth International Congress on Sound and Vibration* (Lisbon, 11–14 July), pp. 191–192 (full paper in CD-ROM Proceedings, Paper 604).

Silvestre, N. and Camotim, D. (2005b). GBT-based local and global vibration analysis of loaded composite thin-walled members, *International Journal of Structural Stability and Dynamics*, **6**(1), in press.

Simão, P. and Silva, L.S. (2004). A unified energy formulation for the stability analysis of open and closed thin-walled members in the framework of the generalized beam theory, *Thin-Walled Structures*, **42**(10), 1495–1517.